



Deposited via The University of Sheffield.

White Rose Research Online URL for this paper:

<https://eprints.whiterose.ac.uk/id/eprint/164462/>

Version: Supplemental Material

Article:

Robshaw, T.J., Griffiths, S.M., Canner, A. et al. (2020) Insights into the interaction of iodide and iodine with Cu(II)-loaded bispicolylamine chelating resin and applications for nuclear waste treatment. *Chemical Engineering Journal*, 390. 124647. ISSN: 1385-8947

<https://doi.org/10.1016/j.cej.2020.124647>

Reuse

This article is distributed under the terms of the Creative Commons Attribution-NonCommercial-NoDerivs (CC BY-NC-ND) licence. This licence only allows you to download this work and share it with others as long as you credit the authors, but you can't change the article in any way or use it commercially. More information and the full terms of the licence here: <https://creativecommons.org/licenses/>

Takedown

If you consider content in White Rose Research Online to be in breach of UK law, please notify us by emailing eprints@whiterose.ac.uk including the URL of the record and the reason for the withdrawal request.

Insights into the interaction of iodide and iodine with Cu(II)-loaded bispicolylamine chelating resins and applications for nuclear waste treatment

Thomas J. Robshaw, Sion M. Griffiths, Adam Canner, James P. Bezzina, Archibald G.L. Waller, Deborah B. Hammond, Sandra van Meurs and Mark D. Ogden

Supporting Information

Table S1. Physical parameters for DOWEX™ M4195 resin, according to manufacturer specification [1].

| Parameter | Value or range |
|--|--------------------------|
| Matrix | Styrene / divinylbenzene |
| Functionality | Bispicolylamine |
| Particle size (mm) | 0.297 – 0.841 |
| Bulk density (kg m ³) | 673 |
| Moisture content (%) | 40 - 60 |
| Cu loading (g L ⁻¹ at pH 2, 6 g.L ⁻¹ feed) | 35 - 42 |

Isotherm models used to fit static equilibrium data

The Langmuir model

The Langmuir isotherm model, (Equation S2) assumes monolayer adsorption over a finite number of degenerate binding sites, with no interaction between adsorbed species.

$$q_e = \frac{q_{\max}K_L C_e}{1+K_L C_e} \quad (\text{Eq. S1})$$

In the Langmuir equation, q_{\max} (mg.g⁻¹) is the theoretical maximal uptake capacity of the adsorbent. K_L is a Langmuir Isotherm constant related to the favorability of adsorption. C_e (mg L⁻¹) is the fluoride concentration in solution at equilibria.

The Freundlich model

The Freundlich isotherm was originally purely an empirical model. However, it is now commonly quoted as being able to describe multilayer adsorption systems where adsorption sites are heterogeneous [2],

$$q_e = K_F C_e^{\frac{1}{n}} \quad (\text{Eq. S2})$$

where K_F and n are Freundlich isotherm constants. K_F is a measure of adsorption capacity and n is a factor of heterogeneity.

The Temkin model

The Temkin isotherm (Equation S4) has been applied to systems where the heat of adsorption decreases linearly as exchange sites are occupied, as a result of interactions between the sorbate species in solution and on the adsorbent surface [3],

$$q_e = \frac{RT}{b_T} \ln (A_T C_e) \quad (\text{Eq. S3})$$

where R is the ideal gas constant (8.314 J.K⁻¹.mol⁻¹), T is temperature (K), b_T is the molar enthalpy of adsorption (kJ.mol⁻¹) and A_T is a Temkin isotherm constant (L.g⁻¹). The term $\frac{RT}{b_T}$ is often represented by a single constant B, related to the heat of adsorption.

The Dubinin-Radushkevich (D-R) model

The D-R isotherm (Equation S5) assumes the adsorption follows a Gaussian distribution of binding energies is used to determine whether chemisorption, ion-exchange or physisorption dominates the system [4],

$$q_e = q_{\max} e^{-B_D \left[RT \ln \left(1 + \frac{1}{C_e} \right) \right]^2} \quad (\text{Eq. S4})$$

where B_D is a D-R isotherm constant (mol² J²). The mean free energy of sorption E_D (J mol⁻¹) can thus be obtained via Equation S6.

$$E_D = \frac{1}{\sqrt{2B_D}} \quad (\text{Eq. S5})$$

Note on the use of the Temkin and D-R isotherms in the determination of total iodine uptake

The average molar concentration of all iodine species present in the mixed iodine/iodide solutions were calculated as follows: For pre-contact solutions, the concentration of iodide only was determined via ISE as previously described. The measured concentrations were compared to that of solutions of pure NaI, which were made up using the same glassware and equivalent masses of NaI salt (accurate to 0.1 mg). The difference in measured [I⁻] between the two sets of solutions was assumed to be due to conversion of a fraction of the original iodide to triiodide, according to the equilibrium I₂ + I⁻ ⇌ I₃⁻. Subsequent measurement of the solutions by ICP-MS allowed for quantification of total iodine species and from this, the apparent [I₂] was calculated. This therefore allowed for a calculation of the molar fractions of iodide, iodine and triiodide in each concentration interval to be carried out. Finally, an average molar mass for all iodine species present in each concentration interval was calculated.

It must be noted that there are two limitations to this technique. The first is that the same determination could not be made for the post-contact solutions and therefore an assumption had to be made that the molar ratios of each species in pre- and post-contact solutions were unity. This may not have been the case. The second is that the technique assumes that iodide, iodine and triiodide were the only species present in significant concentrations and does not take into account the potential formation of polyiodides.

This uncertainty is not significant for Langmuir and Freundlich model-fitting, which does not require the application of molar concentrations. However, results for Temkin and D-R isotherm fitting were accordingly regarded with caution.

Comparison of uptake performance with the literature

Table S2. Comparison of M4195-Cu static iodide uptake performance with other notable ion-exchange resins and metal-loaded adsorbents.

| Adsorbent | Equilibrium uptake capacity (mg g ⁻¹) | Concentration or concentration range (mg L ⁻¹) | Reference |
|--|---|--|------------|
| Duolite A-368 (commercial resin, weak base 3° amine) | 60.3 | 508 | [5] |
| Duolite ARA-9363 (commercial resin, strong base 4° ammonium) | 66.6 | 508 | [5] |
| Ag-doped Cu ₂ O nanoparticles | 25.4 | 2.54-25.4 | [6] |
| Micro/nanostructured Bi ₂ O _{2.33} | 285 | 0.5-700 | [7] |
| CuO/Cu-modified activated carbon | 41.2 | 1-40 | [8] |
| Cu/azurite composite | 136 | 12,700 | [9] |
| Ca alginate/AgCl composite | 152 | 1270 | [10] |
| Lewatit A365 (commercial resin, polyamine) | 589 ± 15 | 1,000-10,000 | [11] |
| Purolite MTS9850 (commercial resin, polyamine) | 761 ± 14 | 1,000-10,000 | [11] |
| M4195-Cu | 305 ± 14 | 50-2,000 | This study |

In all cases, the highest uptake recorded, under optimal conditions, is given.

XRD spectra of spent M4195-Cu samples after iodide uptake at different pHs

Crystalline species are identified as follows: \blacklozenge = CuI, \square = CuO, \circ = Cu₂O.

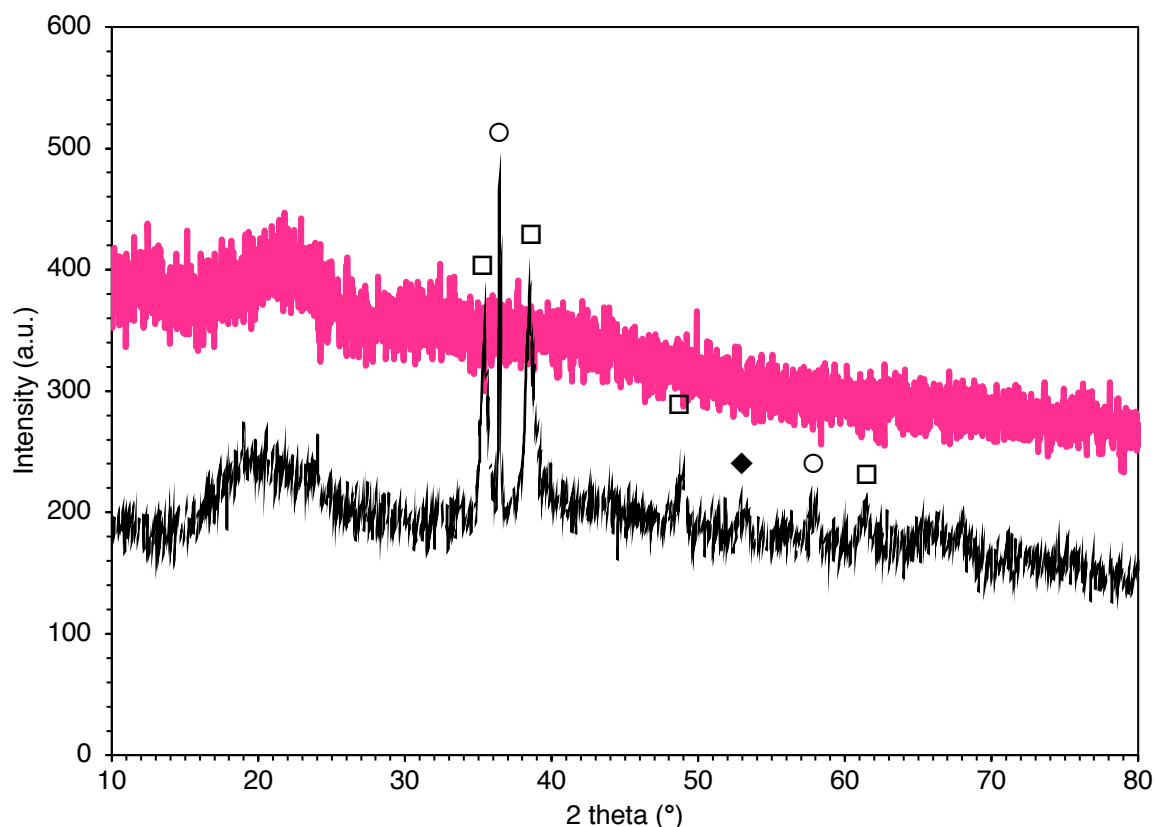


Figure S1. XRD spectra of M4195-Cu after equilibration with NaI solutions at pH 11 (pink line) and pH 12 (black line). Spectra of samples at all other pH values are not shown, but were also completely amorphous.

Investigations into competition effects of nitrate and molybdate

Data treatment

Competition experiments were carried out as described in the main research article. Sample solutions before and after contact with M4195-Cu, were analysed by ion chromatography (see main article experimental) and the uptake of each anion by the resin was determined by mass balancing. The distribution coefficient (K_d) for each anion was calculated as follows:

$$K_d = \frac{\overline{[X^-]}}{[X^-]} \quad (\text{Eq. S6})$$

where $\overline{[X^-]}$ is the concentration of anion immobilized by the polymer (mg g^{-1}) and $[X^-]$ is the concentration remaining in solution at equilibrium (mg mL^{-1}). The separation factor (S.F.) is then calculated from Equation S16:

$$S.F._{(X/Y)} = \frac{K_{d(X)}}{K_{d(Y)}} \quad (\text{Eq. S7})$$

Where X is the ion of interest and Y is a competing ion.

Results

Table S3. Effect of differing cocontaminant molar ratios on uptake of iodide, nitrate and molybdate by M4195-Cu and associated distribution coefficients. Solution volume = 50.0 mL. Sorbent mass = 100 mg. Contact time = 24 hr. T = 20°C. Errors represent 95% confidence intervals from duplicate analyses.

| Molar ratios (I: NO ₃ ⁻ :MoO ₄ ²⁻) | I ⁻ uptake (mg g ⁻¹) | I ⁻ K _d | NO ₃ ⁻ uptake (mg g ⁻¹) | NO ₃ ⁻ K _d | MoO ₄ ²⁻ uptake (mg g ⁻¹) | MoO ₄ ²⁻ K _d |
|--|--|--------------------------------|---|---|---|---|
| 1:0:0 | 27.5 ± 2.1 | 1.49 ± 0.20 × 10 ⁵ | - | - | - | - |
| 1:1:1 | 26.8 ± 3.3 | 1.48 ± 0.20 × 10 ⁵ | 14.1 ± 3.8 | 8.41 ± 1.2 × 10 ⁴ | 41.5 ± 1.8 | 2.15 ± 0.30 × 10 ⁵ |
| 1:2:2 | 24.6 ± 6.0 | 1.45 ± 0.20 × 10 ⁵ | 21.6 ± 6.6 | 6.81 ± 0.89 × 10 ³ | 62.0 ± 3.5 | 3.24 ± 0.45 × 10 ⁵ |
| 1:3:3 | 22.9 ± 3.4 | 2.68 ± 2.0 × 10 ³ | 21.0 ± 1.0 | 3.82 ± 0.21 × 10 ² | 91.5 ± 8.6 | 6.10 ± 5.2 × 10 ³ |
| 1:4:4 | 17.7 ± 2.0 | 2.83 ± 1.5 × 10 ³ | 19.8 ± 3.8 | 3.41 ± 1.3 × 10 ² | 115 ± 4.4 | 20.2 ± 2.5 × 10 ³ |
| 1:5:5 | 15.3 ± 2.8 | 1.17 ± 0.80 × 10 ³ | 21.0 ± 1.5 | 2.44 ± 0.14 × 10 ² | 123 ± 20 | 1.82 ± 1.8 × 10 ³ |
| 1:6:6 | 18.6 ± 1.8 | 1.24 ± 0.07 × 10 ³ | 16.5 ± 0.6 | 1.32 ± 0.03 × 10 ² | 160 ± 5 | 2.79 ± 1.3 × 10 ³ |
| 1:7:7 | 15.6 ± 1.7 | 0.841 ± 0.24 × 10 ³ | 22.3 ± 4.8 | 1.70 ± 0.45 × 10 ² | 130 ± 19 | 0.646 ± 0.10 × 10 ³ |
| 1:8:8 | 18.5 ± 1.9 | 1.27 ± 0.18 × 10 ³ | 15.8 ± 5.4 | 0.90 ± 0.34 × 10 ² | 162 ± 36 | 1.11 ± 1.0 × 10 ³ |
| 1:9:9 | 15.6 ± 3.5 | 0.782 ± 0.36 × 10 ³ | 25.0 ± 5.5 | 1.34 ± 0.35 × 10 ² | 185 ± 44 | 0.802 ± 0.458 × 10 ³ |
| 1:10:10 | 15.1 ± 0.3 | 0.695 ± 0.27 × 10 ³ | 28.3 ± 9.4 | 1.28 ± 0.62 × 10 ² | 186 ± 44 | 0.604 ± 0.346 × 10 ³ |

Table S4. Determined separation factors (S.F.s) for iodide verses the two cocontaminants. All experimental conditions as per Table S3.

| Molar ratios (I:NO ₃ ⁻ :MoO ₄ ²⁻) | S.F. (I/NO ₃ ⁻) | S.F. (I/MoO ₄ ²⁻) |
|---|--|--|
| 1:0:0 | - | - |
| 1:1:1 | 4.88 ± 2.22 | 1.04 ± 0.25 |
| 1:2:2 | 13.5 ± 6.0 | 0.642 ± 0.14 |
| 1:3:3 | 6.87 ± 2.52 | 0.460 ± 0.025 |
| 1:4:4 | 8.05 ± 0.66 | 0.449 ± 0.24 |
| 1:5:5 | 4.90 ± 1.78 | 0.816 ± 0.18 |
| 1:6:6 | 9.44 ± 0.13 | 0.494 ± 0.10 |
| 1:7:7 | 5.31 ± 1.42 | 1.35 ± 0.29 |
| 1:8:8 | 15.6 ± 4.0 | 2.07 ± 1.02 |
| 1:9:9 | 6.39 ± 2.16 | 1.01 ± 0.07 |
| 1:10:10 | 6.72 ± 2.69 | 1.22 ± 0.12 |

Dynamic breakthrough models

The Modified Dose-Response model

$$\frac{c}{c_i} = 1 - \frac{1}{1 + \left(\frac{V_{\text{eff}}}{b}\right)^a} \quad (\text{Eq. S8})$$

$$q_0 = \frac{bc_i}{m} \quad (\text{Eq. S9})$$

The Dose-Response model was first used to describe biosorption of heavy metals [12], but has been proven to be useful in modelling the uptake of a range of contaminants via ion-exchange adsorbents [13, 14]. In these equations V_{eff} is the volume of solution eluted from the column (mL), a and b are constants of the Dose-Response model, q_0 is the theoretical

maximum uptake capacity of the resin in a dynamic environment ($\text{mg}\cdot\text{g}^{-1}$) and m is the dry mass of resin (g).

The Adams-Bohart (AB) model

$$\frac{C}{C_i} = \frac{1}{1 + e^{\left(\frac{k_{AB}}{Q}\right)(q_0 m - C_i V_{\text{eff}})}} \quad (\text{Eq. S10})$$

This model assumes an irreversible adsorption isotherm and does not consider intra-particle diffusion processes. It should be noted that the AB model, given in this simplified form, is often incorrectly cited as the Thomas model and data which fits the equation is assumed to represent a system controlled by 2nd-order kinetics, with the rate-limiting step being interfacial mass-transfer. Chu showed that the actual Thomas model is more complicated and assumes a Langmuir adsorption isotherm. However, when adsorption is particularly favourable, the Thomas model simplifies to the AB model and these assumptions may be valid [15]. In Eq. S10, C = concentration of the species of interest in the effluent at a given time ($\text{mg}\cdot\text{L}^{-1}$), C_i = concentration in the inlet to the column ($\text{mg}\cdot\text{L}^{-1}$), k_{AB} = Adams-Bohart rate constant ($\text{mL}\cdot\text{min}^{-1}\cdot\text{mg}^{-1}$), Q = flow rate ($\text{mL}\cdot\text{min}^{-1}$), q_0 = theoretical maximum capacity of the resin on a dry mass basis ($\text{mg}\cdot\text{g}^{-1}$) m = dry mass of resin in column (g) and V_{eff} = volume of effluent (mL).

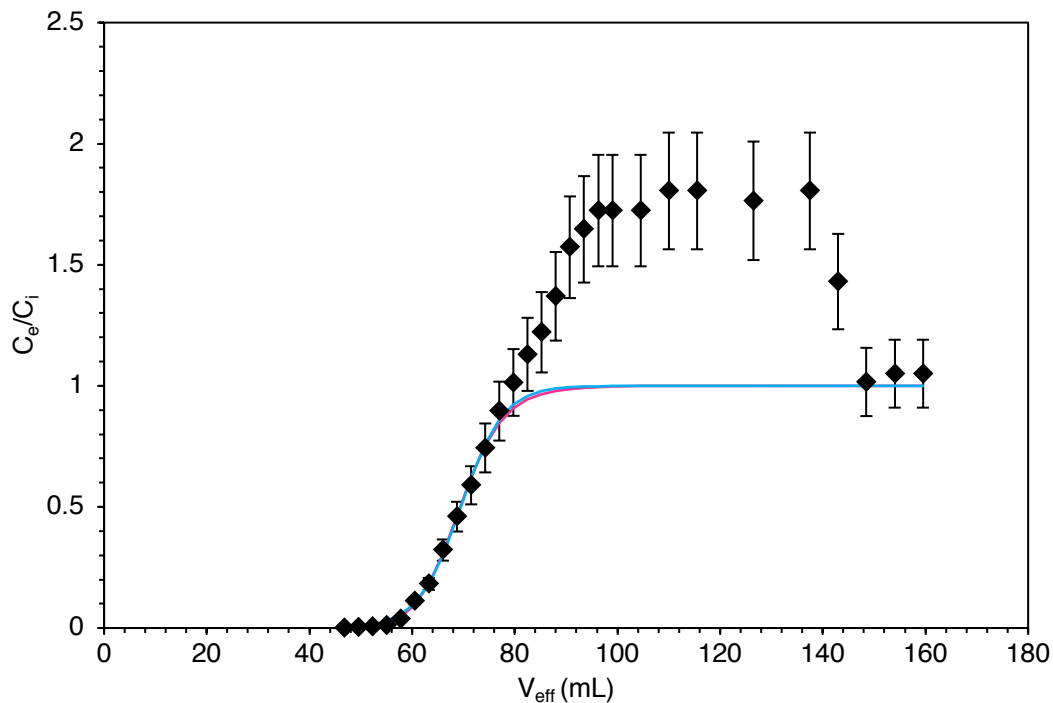


Figure S2. Breakthrough curve for Purolite MTS9850 with iodide, 10 meq nitrate and 10 meq molybdate solution, fitted to the Dose-Response (pink line) and Adams-Bohart (blue line) dynamic breakthrough models. Resin BV = 5.50 mL. Inlet $[\text{I}^-] = 2.00 \text{ g}\cdot\text{L}^{-1}$. Flow rate = 1 BV \cdot hr $^{-1}$. $T = 20^\circ\text{C}$. Error bars represent the approximate 95 % confidence intervals, derived from 3 x electrode measurements.

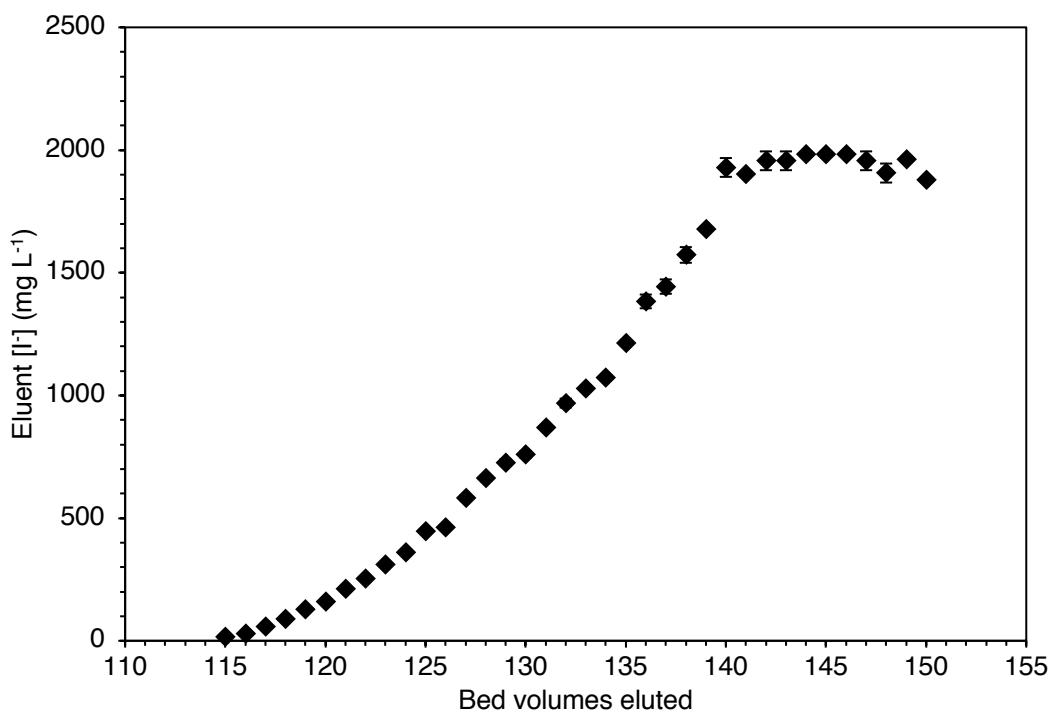
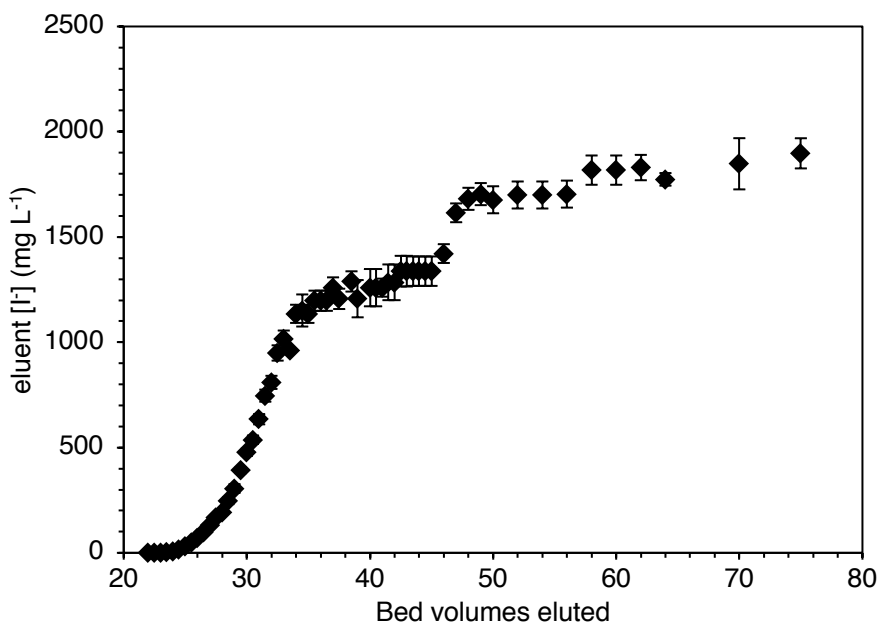


Figure S3. Raw data for M4195-Cu column loading and breakthrough experiment with iodide only solution. Resin BV = 5.50 mL. Inlet [I⁻] = 2.00 g.L⁻¹. Flow rate = 1 BV.hr⁻¹. T = 20°C. Error bars represent the approximate 95 % confidence intervals, derived from 3 x electrode measurements.



peak assignments are displayed in Tables S5-6. Assignments were based on the studies of Green *et al.* [16], Refat *et al.* [17] and Wang *et al.* [18]

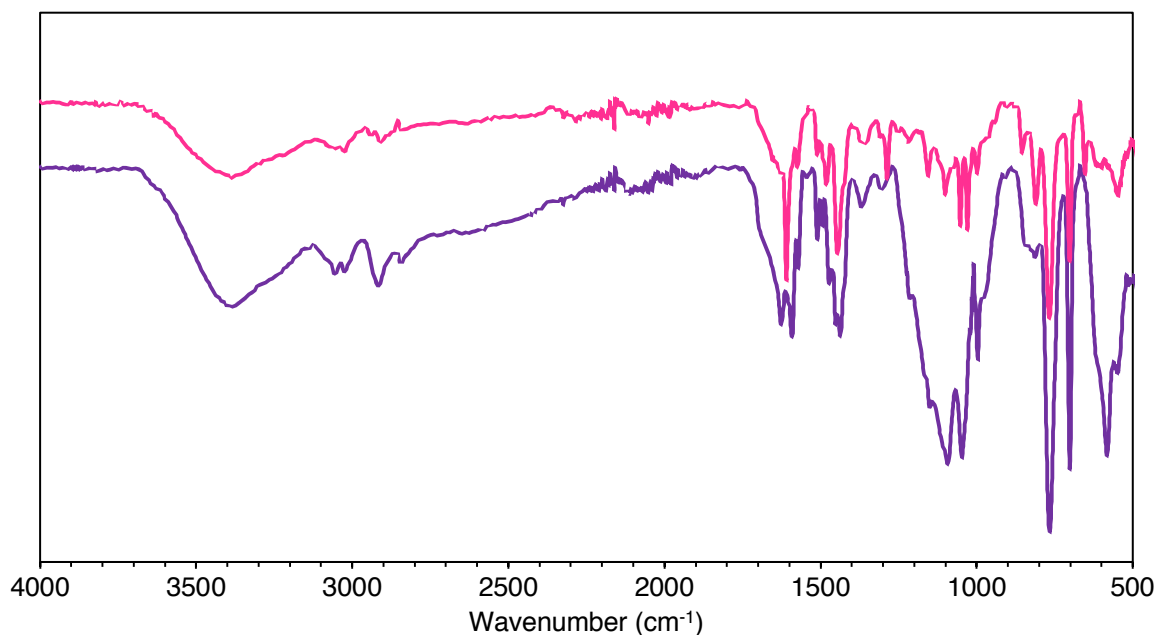


Figure S5. FTIR spectrum of M4195 resin, as-delivered by the manufacturer (purple line) and M4195-Cu (pink line)

Table S5. Assignment of FTIR spectral peaks for M4195 resin.

| Peak | Assignment |
|-----------------|---|
| 3386 | N-H st. |
| 3055 and 3021 | Aromatic C-H st. |
| 2911 and 2841 | Aliphatic C-H st. |
| 1685 (shoulder) | N-H bend |
| 1627 | Pyridyl C=N st. |
| 1590 | Pyridyl C=C st. |
| 1571 | Phenyl C=C st. |
| 1511 | Phenyl C=C st. |
| 1471 | Pyridyl C=C st. |
| 1436 | sp ³ C-H bend (-CH ₂ -) |
| 1370 | Sulfate S=O st. |
| 1298 | Aliphatic C-N st. |
| 1094 | Pyridyl ring breathing, in-plane |
| 1047 | Pyridyl ring breathing, in-plane |
| 996 | Phenyl ring breathing, in-plane |
| 767 | Pyridyl C-H sp ² bend (mono substituted), out-of-plane |
| 702 | Phenyl C-H sp ² bend (mono substituted), out-of-plane |
| 584 | Ring deformation |

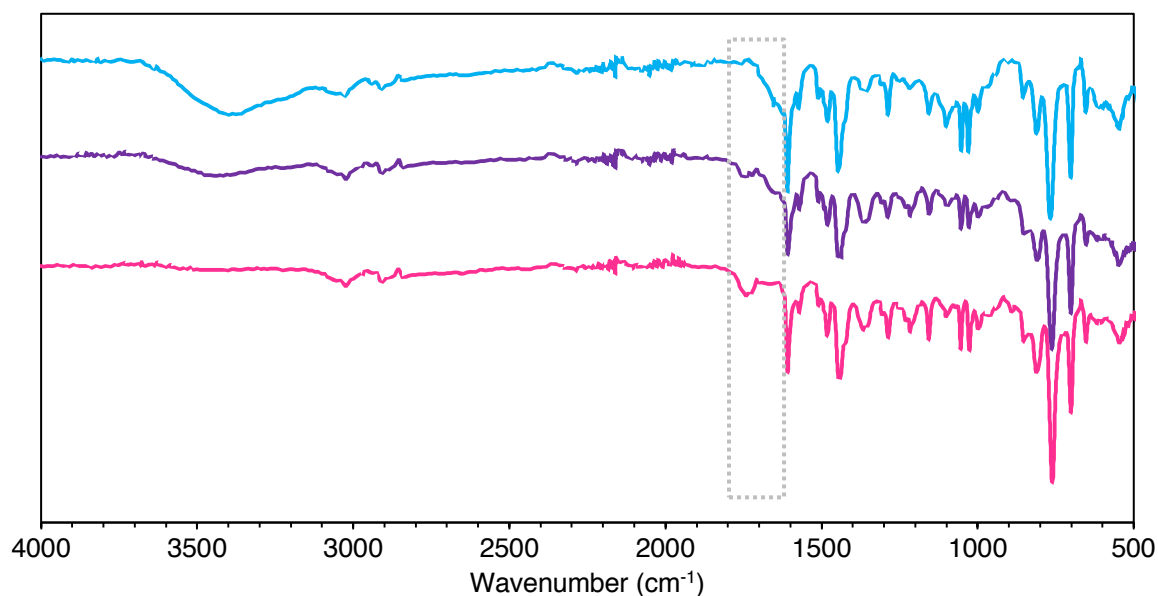


Figure S6. FTIR spectrum of M4195-Cu resin (blue line). M4195-Cu after equilibrium contact with $1.00 \text{ g L}^{-1} \text{ I}^-$ (purple line) and M4195-Cu after equilibrium contact with $1.00 \text{ g L}^{-1} \text{ I}^-$ and 6 molar equivalents organic I_2 . N-H bend region highlighted.

Table S6. Assignment of FTIR spectral peaks for M4195-Cu resin samples from Fig. S6.

| Peak | Assignment |
|------------------------------------|---|
| 3386 | N-H st. and O-H st. |
| 3023 | Aromatic C-H st. |
| 2908 | Aliphatic C-H st. |
| 1739 (iodine treated samples only) | Unknown |
| 1688 (shoulder) | N-H bend (intensity reduced upon iodine contact) |
| 1610 | Pyridyl C=N st. |
| 1573 | Phenyl C=C st. |
| 1481 | Pyridyl C=C st. |
| 1445 | sp^3 C-H bend ($-\text{CH}_2-$) |
| 1287 | Aliphatic C-N st. |
| 1156 | Aliphatic C-N st. |
| 1101 | Pyridyl ring breathing, in-plane |
| 1052 and 1030 | Pyridyl ring breathing, in-plane |
| 998 | Phenyl ring breathing in-plane |
| 854 | Phenyl group sp^2 bend (paradisubstituted), out-of-plane |
| 812 | Phenyl group sp^2 bend (paradisubstituted), out-of-plane |
| 767 | Pyridyl C-H sp^2 bend (mono substituted), out-of-plane |
| 702 | Phenyl C-H sp^2 bend (mono substituted), out-of-plane |
| 653 | Ring deformation |
| 546 | Ring deformation |

Additional FTIR spectra were produced, using the KBr disk method, for better visualisation of the C-H st. region, which show the decrease in relative intensity of the C-H st. peaks for M4195-Cu samples treated with iodide and iodine. It is seen in the figure below that for the pre-contact sample, the C-H st. is close to the same intensity as the aromatic C=C st., whereas for the post-contact sample, it is relatively weaker.

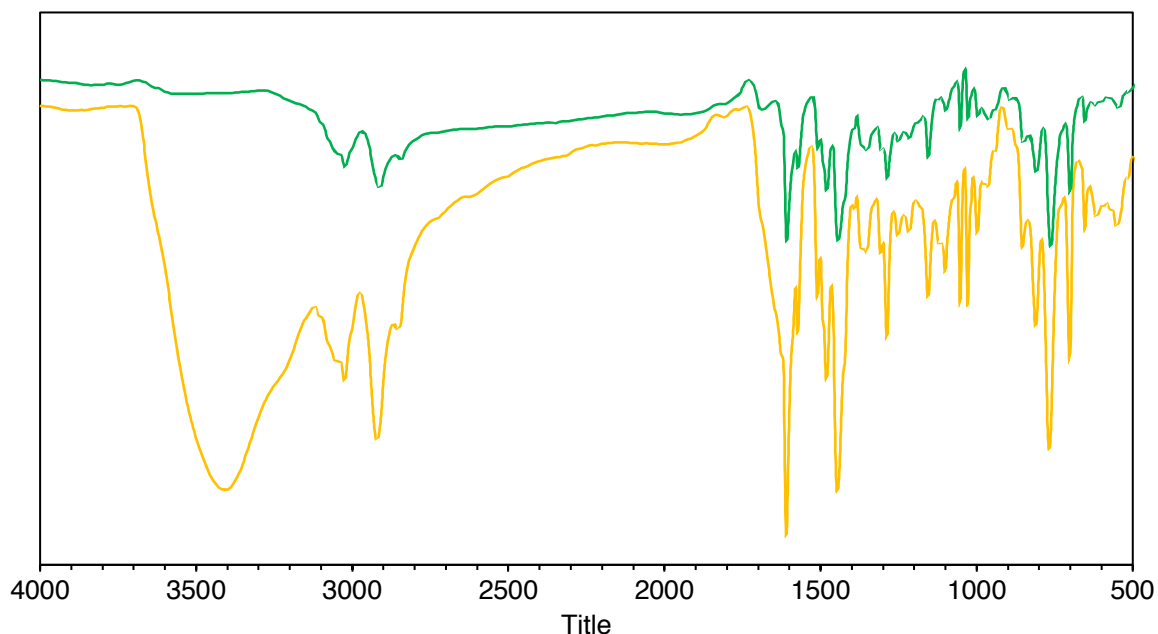


Figure S7. KBr FTIR spectrum of M4195-Cu (yellow line) and M4195-Cu after equilibrium contact with 1.00 g.L⁻¹ I⁻ and 6 molar equivalents organic I₂ (green line).

Determination of deprotonation via iodide- and iodine-loading

A number of batch equilibrium experiments were conducted, as described in the main research article, with both iodide and mixed iodide/iodine systems. In all cases, the pH of the contact solution was measured before and after equilibration.

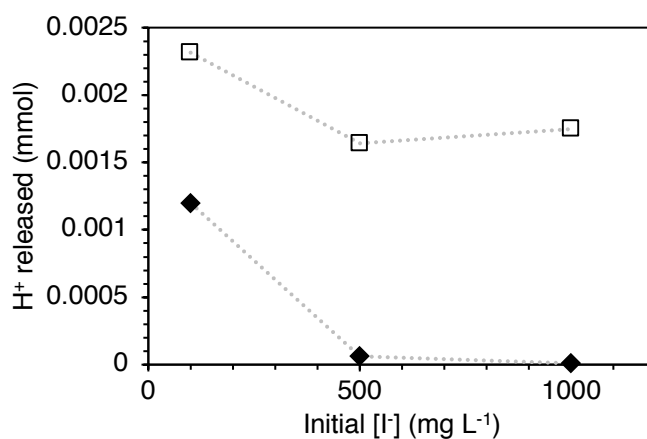


Figure S8. Release of protons into solution from contact of 1 g.L⁻¹ iodide (◆) and 1 g.L⁻¹ iodide with 6 molar equivalents iodine (□) with M4195-Cu. Error values (95% confidence intervals) derived from 3 x electrode measurements, but are too small to be graphically represented. Solution volume = 50.0 mL. Sorbent mass = 100 mg. Contact time = 24 hr. T = 20°C.

RAMAN characterisation

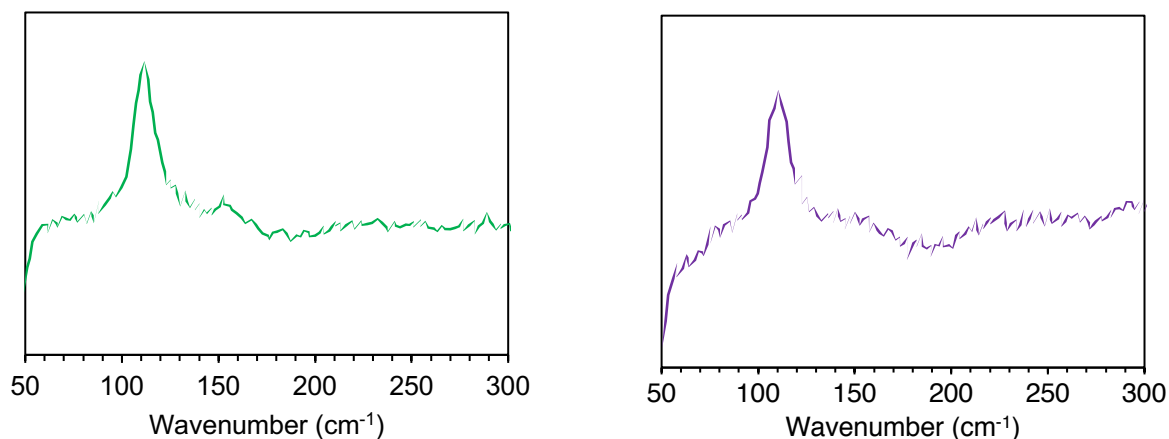


Figure S9. RAMAN spectra of M4195-Cu after equilibrium contact with 1.00 g.L⁻¹ I⁻ (left) and M4195-Cu after equilibrium contact with 1.00 g.L⁻¹ I⁻ and 6 molar equivalents organic I₂ (right).

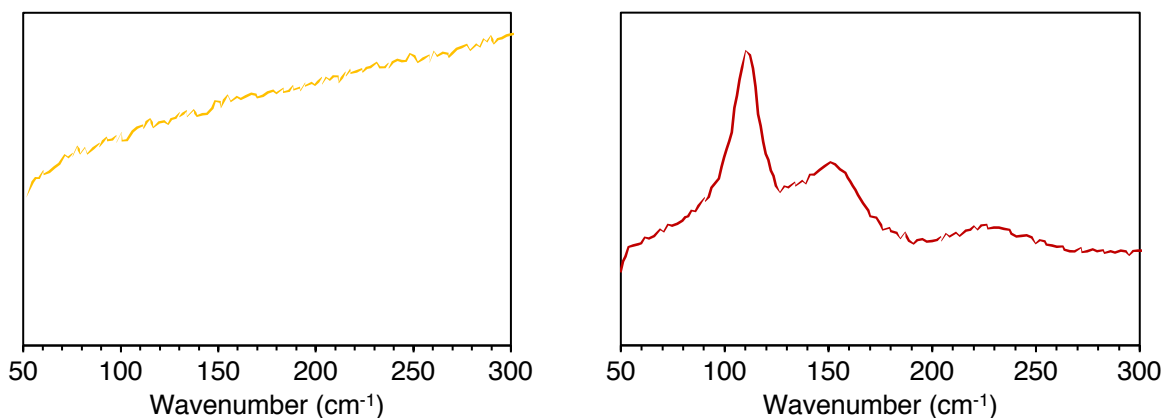


Figure S10. RAMAN spectra of MTS9850 after equilibrium contact with 1.00 g.L⁻¹ I⁻ (left) and MTS9850 after equilibrium contact with 1.00 g.L⁻¹ I⁻ and 6 molar equivalents organic I₂ (right).

Solid state NMR characterization

Experimental

Solid-State NMR samples were packed into 4 mm zirconia rotors and transferred to a Bruker Avance III HD spectrometer. 1D ¹H-¹³C and ¹H-¹⁵N cross-polarisation magic angle spinning (CP/MAS) NMR experiments were measured at 500 (¹H), 126 (¹³C) and 50.8 (¹⁵N) MHz at the MAS rate of 10.0 kHz. The ¹H $\pi/2$ pulse was 3.4 μ s, and two-pulse phase modulation (TPPM) decoupling was used during the acquisition. The Hartmann-Hahn condition was set using hexamethylbenzene. The spectra were measured using a contact time of 2.0 ms. The relaxation delay D_1 for each sample was individually determined from the proton T_1 measurement ($D_1 = 5 \times T_1$). Samples were collected until sufficient signal to noise was

observed, typically greater than 256 scans. The values of the chemical shifts are referred to that of TMS.

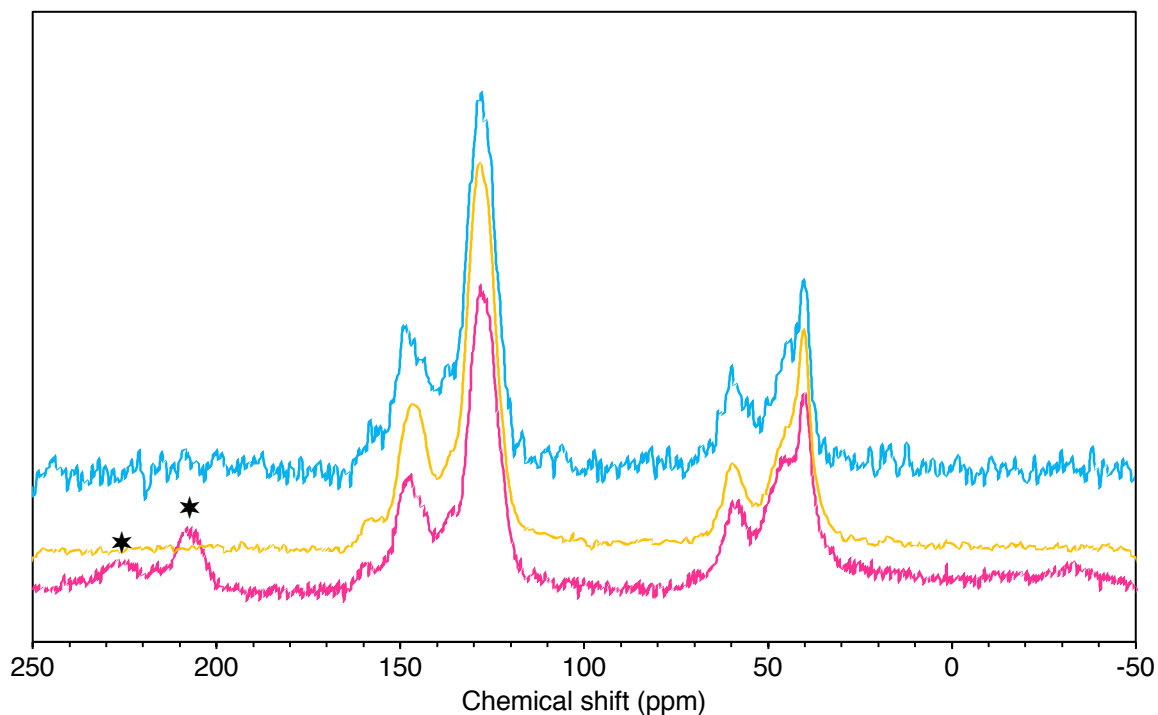


Figure S11. ¹³C solid state NMR spectrum of M4195 (pink line), M4195 after equilibrium contact with 1.00 g.L⁻¹ I⁻ (yellow line) and M4195 after equilibrium contact with 1.00 g.L⁻¹ I⁻ and 6 molar equivalents organic I₂ (blue line). * = spinning side bands.

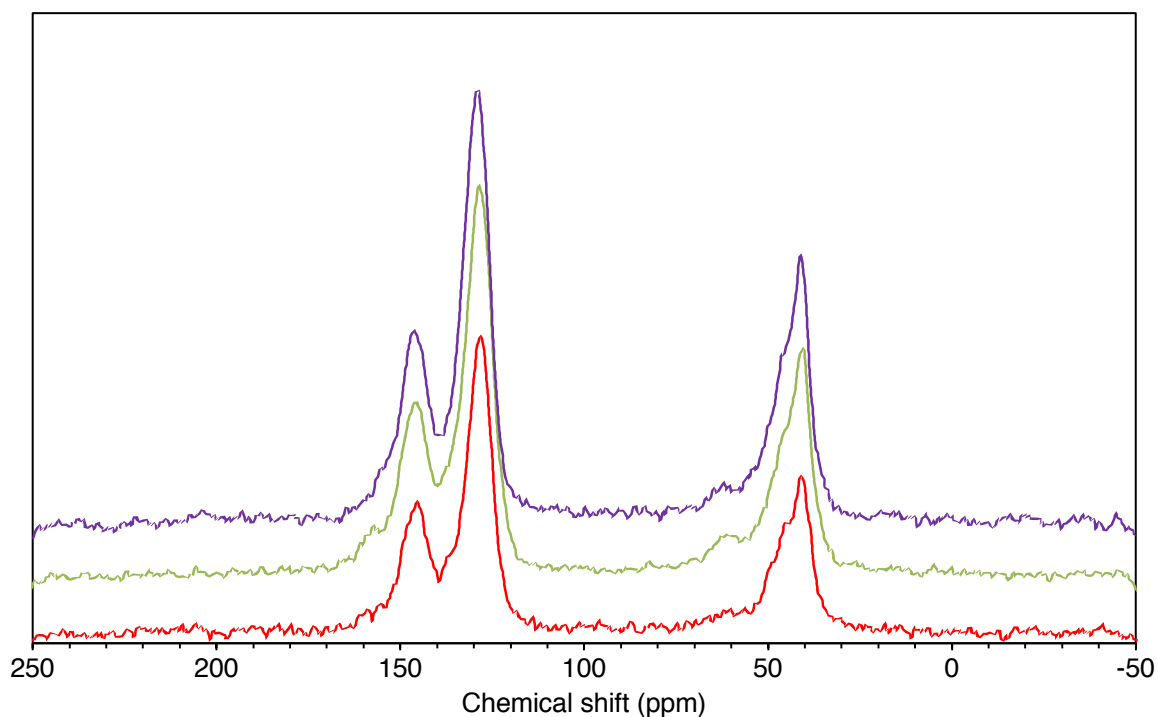


Figure S12. ¹³C solid state NMR spectrum of M4195-Cu (red line), M4195-Cu after equilibrium contact with 1.00 g.L⁻¹ I⁻ (green line) and M4195-Cu after equilibrium contact with 1.00 g.L⁻¹ I⁻ and 6 molar equivalents organic I₂ (purple line).

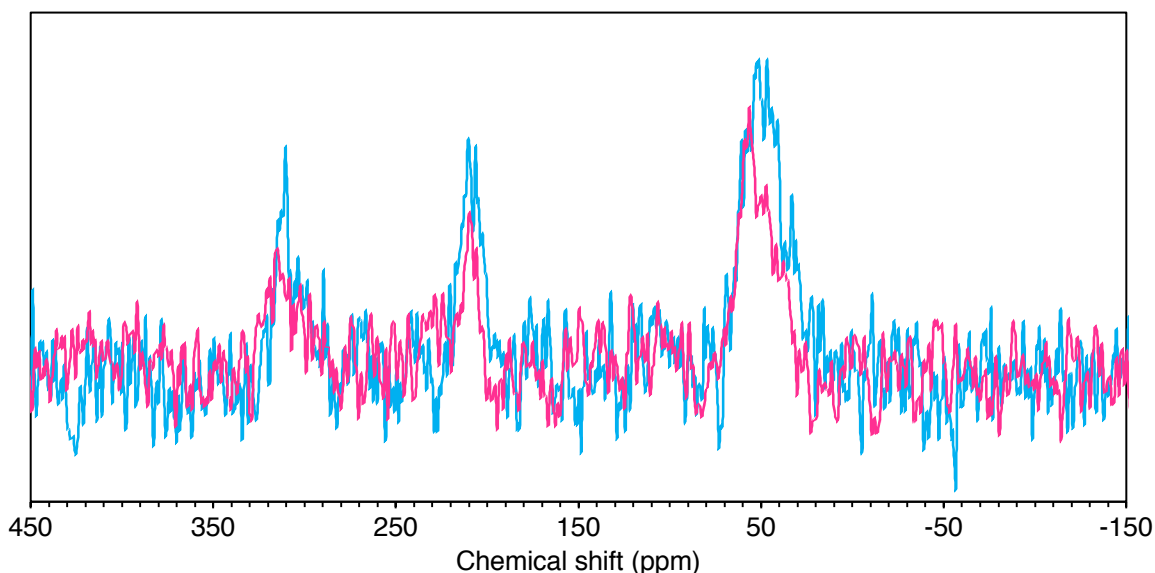


Figure S13. ^{15}N solid state NMR spectrum of M4195 (pink line) and M4195 after equilibrium contact with $1.00 \text{ g.L}^{-1} \text{ I}^-$ and 6 molar equivalents organic I_2 (blue line).

XPS characterization

Experimental

Samples were all prepared by pushing the submitted powders into indium foil.

The analyses were carried out using a Kratos Supra instrument with a monochromated aluminium source and two analysis points per sample. The analysis area was $700 \mu\text{m}$ by $300 \mu\text{m}$. Charge neutralisation was used throughout. The survey scans were collected between $1200\text{-}0 \text{ eV}$, at 1 eV energy resolution, and two 300 second sweeps. High resolution O 1s, C 1s, N 1s, S 2p and, where appropriate, Cu 2p, I 3d, Cl 2p, Mo 3d and Cu Auger scans were collected over an appropriate energy range at 0.1 eV energy resolution.

The data collected was calibrated in intensity using a transmission function characteristic of the instrument (determined using software from NPL) to make the values instrument-independent. The data was then quantified using theoretical Schofield relative sensitivity factors. All data was calibrated relative to a C 1s position of 285.0 eV for C-C/C-H type carbon environments.

Post-contact samples were produced by contacting 100 mg of M4195-Cu with 50 mL contact solution. For all iodide-treated samples, initial $[\text{I}^-]$ was 1.0 g.L^{-1} . For I^-/I_2^- treated samples, 6 molar equivalents organic I_2 was used. For cocontaminant-treated samples, 10 molar equivalents NO_3^- and 10 molar equivalents MoO_4^{2-} were used.

Table S7. Surface composition (atomic %) of M4195 samples at various processing stages, determined by quantifying XPS surface scans.

| Sample | Cu | I | O | In | N | C | Mo | Cl | S | Si |
|---|------|-----|-----|------|------|------|------|------|------|------|
| M4195 a | <0.1 | 0.1 | 6.6 | <0.1 | 8.4 | 83.4 | <0.1 | <0.1 | 1.4 | 0.2 |
| M4195 b | <0.1 | 0.1 | 7.1 | 0.6 | 8.2 | 82.5 | <0.1 | <0.1 | 1.3 | 0.2 |
| M4195-Cu a | 1.9 | 0.4 | 7.6 | 3.6 | 6.8 | 75.8 | <0.1 | 3.8 | 0.2 | 0.1 |
| M4195-Cu b | 2.1 | 0.4 | 3.0 | <0.1 | 8.8 | 81.2 | <0.1 | 4.2 | 0.2 | <0.1 |
| M4195-Cu + I ⁻ a | 3.8 | 4.8 | 3.0 | <0.1 | 8.6 | 79.6 | <0.1 | 0.3 | <0.1 | <0.1 |
| M4195-Cu + I ⁻ b | 3.8 | 4.9 | 2.4 | <0.1 | 8.5 | 80.1 | <0.1 | 0.4 | <0.1 | <0.1 |
| M4195-Cu + I ⁻ + I ₂ a | 4.2 | 5.4 | 4.0 | 1.4 | 8.0 | 76.3 | <0.1 | 0.7 | <0.1 | <0.1 |
| M4195-Cu + I ⁻ + I ₂ b | 4.5 | 5.9 | 2.2 | 0.0 | 8.6 | 78.2 | <0.1 | 0.6 | 0.1 | <0.1 |
| M4195-Cu + I ⁻ + I ₂ c | 4.2 | 5.3 | 4.2 | 1.8 | 7.8 | 76.0 | <0.1 | 0.7 | <0.1 | <0.1 |
| M4195-Cu + I ⁻ + NO ₃ ⁻ + MoO ₄ ²⁻ a | 3.0 | 2.4 | 6.4 | <0.1 | 11.6 | 74.4 | 1.4 | 0.2 | <0.1 | 0.6 |
| M4195-Cu + I ⁻ + NO ₃ ⁻ + MoO ₄ ²⁻ b | 3.3 | 2.6 | 9.0 | 1.1 | 13.6 | 67.9 | 1.5 | 0.3 | <0.1 | 0.6 |
| M4195-Cu + I ⁻ + NO ₃ ⁻ + MoO ₄ ²⁻ c | 2.8 | 2.1 | 7.2 | 0.1 | 11.4 | 74.7 | 1.4 | <0.1 | <0.1 | 0.3 |

Notes: Samples where substantial In/Si contamination was observed were run in triplicate. The N % in the cocontaminant-treated samples includes a contribution from suspected Mo 2p satellites.

Table S8. Results of curve-fitting of high-resolution N 1s scans. B.E. = binding energy. Suspected Mo 2p satellites not presented.

| Sample | Environment | | | | | |
|---|-------------|----------|----------------------|----------|-----------|----------|
| | Pyridyl | | Quarternary ammonium | | Nitrate | |
| | B.E. (eV) | %At Conc | B.E. (eV) | %At Conc | B.E. (eV) | %At Conc |
| M4195 a | 398.4 | 82.4 | 400.7 | 17.6 | | |
| M4195 b | 398.5 | 79.9 | 400.8 | 20.2 | | |
| M4195-Cu a | 399.1 | 93.5 | 401.4 | 6.5 | | |
| M4195-Cu b | 399.1 | 93.6 | 401.6 | 6.4 | | |
| M4195-Cu c | 399.0 | 91.5 | 401.5 | 8.5 | | |
| M4195-Cu + I ⁻ a | 399.1 | 94.9 | 401.3 | 5.1 | | |
| M4195-Cu + I ⁻ b | 399.1 | 94.7 | 401.4 | 5.3 | | |
| M4195-Cu + I ⁻ + I ₂ a | 399.3 | 93.0 | 401.5 | 7.0 | | |
| M4195-Cu + I ⁻ + I ₂ b | 399.3 | 92.5 | 401.5 | 7.6 | | |
| M4195-Cu + I ⁻ + I ₂ c | 399.3 | 90.1 | 401.5 | 9.9 | | |
| M4195-Cu + I ⁻ + NO ₃ ⁻ + MoO ₄ ²⁻ a | 399.2 | 85.9 | 401.4 | 6.9 | 405.8 | 7.1 |
| M4195-Cu + I ⁻ + NO ₃ ⁻ + MoO ₄ ²⁻ b | 399.2 | 85.3 | 401.1 | 8.5 | 405.7 | 6.2 |
| M4195-Cu + I ⁻ + NO ₃ ⁻ + MoO ₄ ²⁻ c | 399.2 | 87.3 | 401.4 | 6.2 | 405.7 | 6.6 |

Table S9. Results of curve-fitting of high-resolution Cu 2p scans. L = bispicolyamine ligand.

| Sample | Environment | | | | | | | | |
|---|---------------------|----------|----------------------|----------|-----------|----------|-----------|----------|-----------|
| | Cu(I)L ₂ | | Cu(II)L ₂ | | Cu(I)L | | Cu(II)L | | Satellite |
| | B.E. (eV) | %At Conc | B.E. (eV) | %At Conc | B.E. (eV) | %At Conc | B.E. (eV) | %At Conc | %At Conc |
| M4195-Cu a | | | 931.7 | 13.1 | | | 933.7 | 52.5 | 34.4 |
| M4195-Cu b | | | 931.8 | 15.7 | | | 933.8 | 47.9 | 36.5 |
| M4195-Cu + I ⁻ a | 928.7 | 13.6 | | | 931.1 | 35.7 | 933.7 | 30.9 | 19.8 |
| M4195-Cu + I ⁻ b | 928.7 | 13.4 | | | 931.2 | 37.0 | 933.7 | 30.0 | 19.6 |
| M4195-Cu + I ⁻ + I ₂ a | 929.1 | 14.3 | | | 931.1 | 25.2 | 933.8 | 36.2 | 24.3 |
| M4195-Cu + I ⁻ + I ₂ b | 928.9 | 13.3 | | | 931.1 | 27.2 | 933.7 | 35.3 | 24.3 |
| M4195-Cu + I ⁻ + NO ₃ ⁻ + MoO ₄ ²⁻ a | 928.8 | 6.9 | | | 931.2 | 31.8 | 933.8 | 33.3 | 28.0 |
| M4195-Cu + I ⁻ + NO ₃ ⁻ + MoO ₄ ²⁻ b | 928.7 | 7.8 | | | 931.2 | 34.9 | 933.7 | 33.7 | 23.7 |

Table S10. Results of curve-fitting of high-resolution I 3d^{5/2} scans. L = bispicolyamine ligand.

| Sample | Environment | | | |
|---|-------------|----------|-----------------------|----------|
| | Iodide | | Triiodide (tentative) | |
| | B.E. (eV) | %At Conc | B.E. (eV) | %At Conc |
| M4195-Cu + I ⁻ a | 617.9 | 94.4 | 619.7 | 5.6 |
| M4195-Cu + I ⁻ b | 618.0 | 94.6 | 619.7 | 5.4 |
| M4195-Cu + I ⁻ + I ₂ a | 618.1 | 88.9 | 619.6 | 11.1 |
| M4195-Cu + I ⁻ + I ₂ b | 618.2 | 90.4 | 619.7 | 9.6 |
| M4195-Cu + I ⁻ + I ₂ c | 618.1 | 87.7 | 619.6 | 12.3 |
| M4195-Cu + I ⁻ + NO ₃ ⁻ + MoO ₄ ²⁻ a | 618.0 | 93.2 | 619.5 | 6.8 |
| M4195-Cu + I ⁻ + NO ₃ ⁻ + MoO ₄ ²⁻ b | 618.1 | 90.0 | 619.7 | 10.0 |
| M4195-Cu + I ⁻ + NO ₃ ⁻ + MoO ₄ ²⁻ c | 618.1 | 96.1 | 620.1 | 3.9 |

UV-vis spectra of desorbed iodine species

Experimental

5.0 mg of resin, at various process stages, was contacted with 5.0 mL methanol. These were sealed in a glass scintillation vial and agitated, via orbital shaker for 8 hr. The resulting solution was diluted to appropriate concentration, if necessary, and analysed as described in the main research article. For reference, the spectra of pure NaI and I₂ were also collected. We also contacted a further NaI sample with a 20 μL spike of concentrated HNO₃, to form the triiodide in solution for analysis.

Results

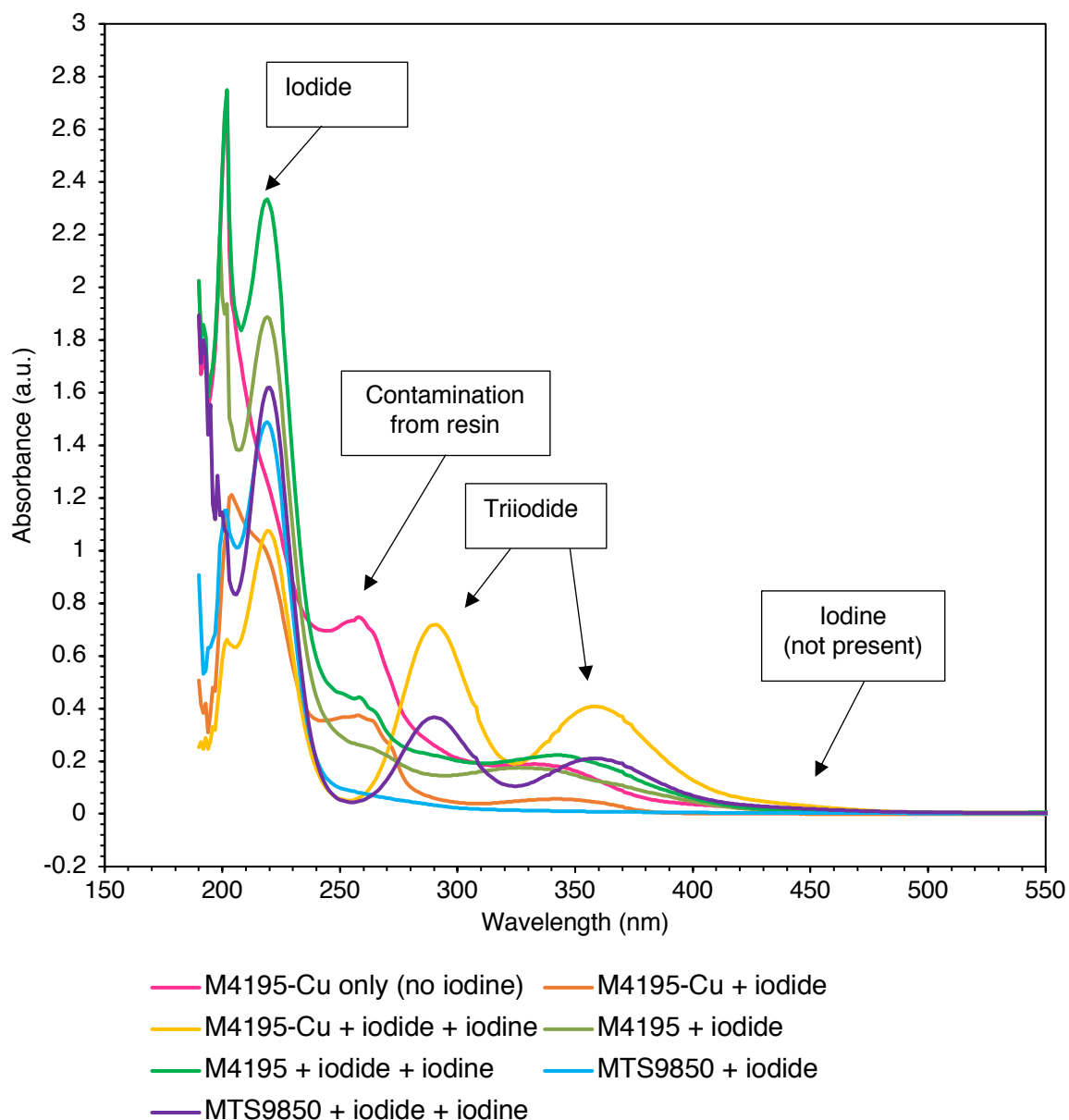


Figure S14. UV-vis spectra of attempted back extraction of iodine species into methanol from spent resin samples. M4195-Cu + iodide was diluted by a factor of 2. M4195-Cu + iodide + iodine was diluted by a factor of 100. All other samples undiluted. In the original NaI contact solution, initial $[I^-]$ was 1.00 g L^{-1} and in the original NaI/I₂ contact solution, initial $[I^-]$ was 1.00 g.L^{-1} with 6 molar equivalents I₂.

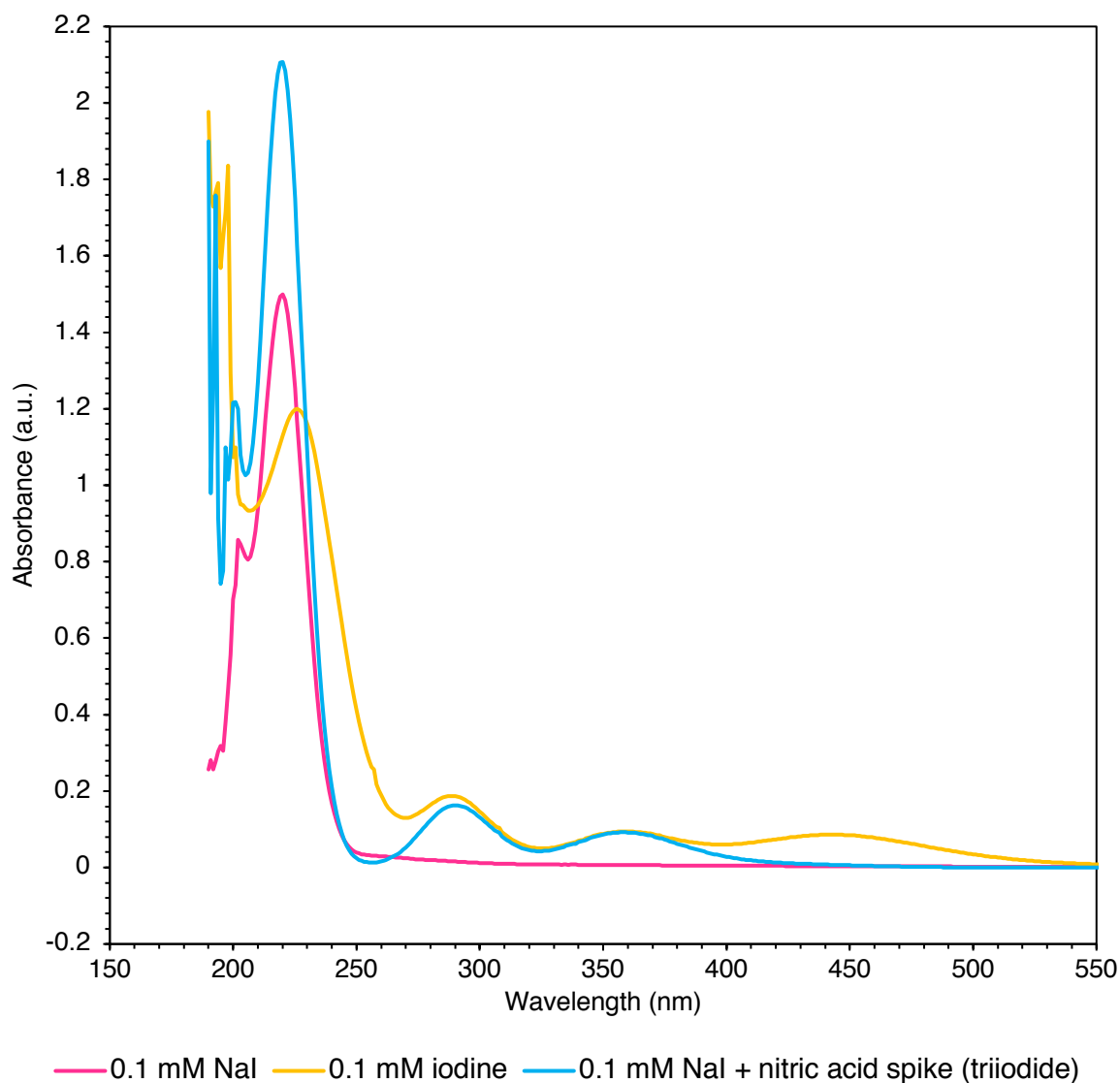


Figure S15. UV-vis spectra of iodine species in solution, made by dissolution of analytical reagents, for comparison to S14.

XRD spectra of combusted and partially-combusted resin samples

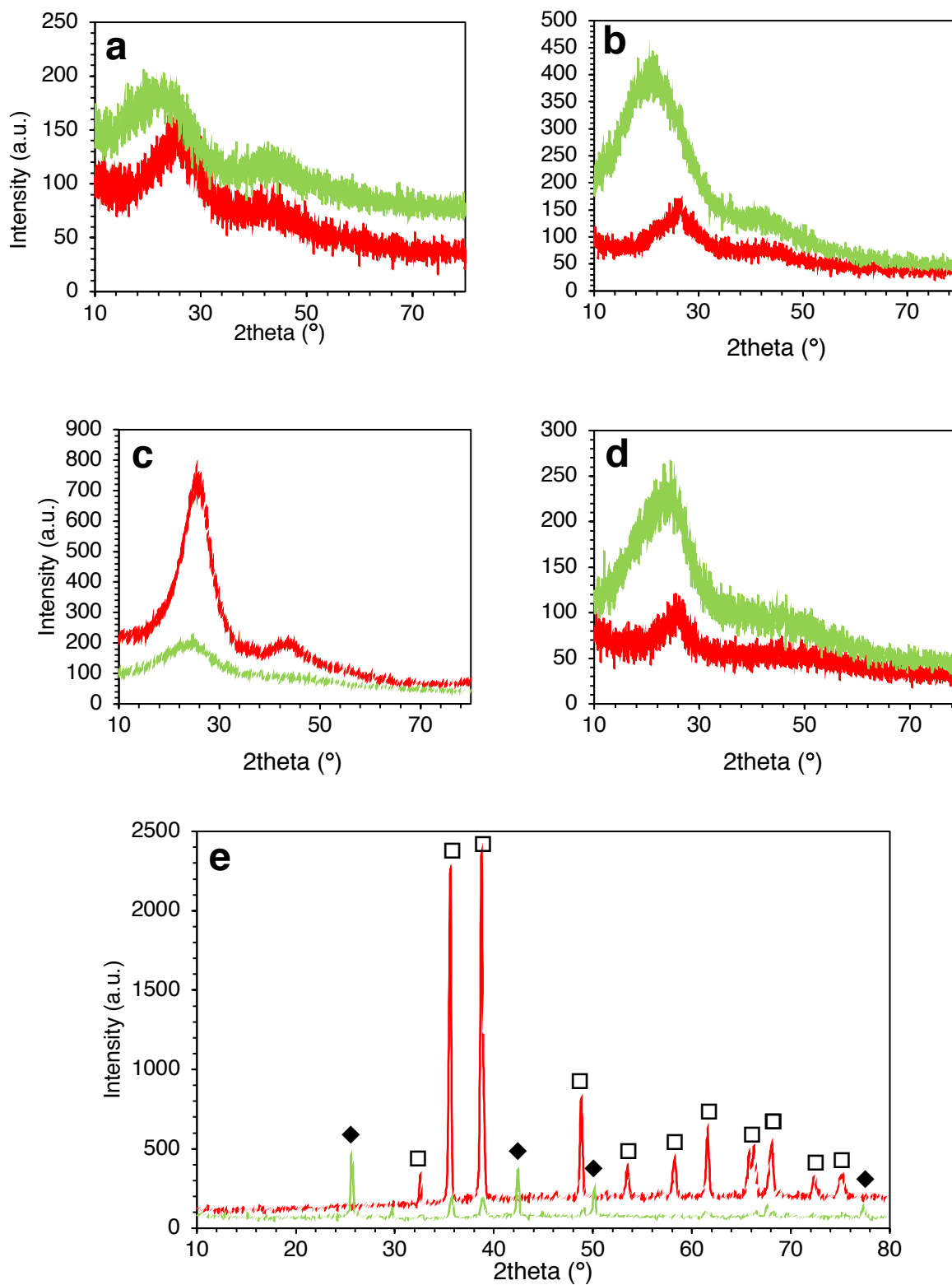
Experimental

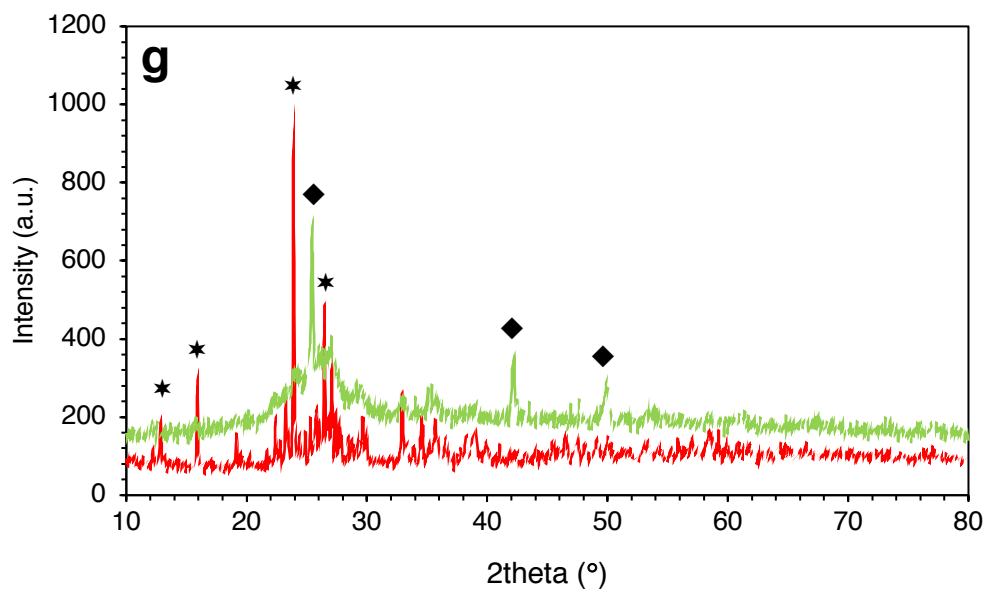
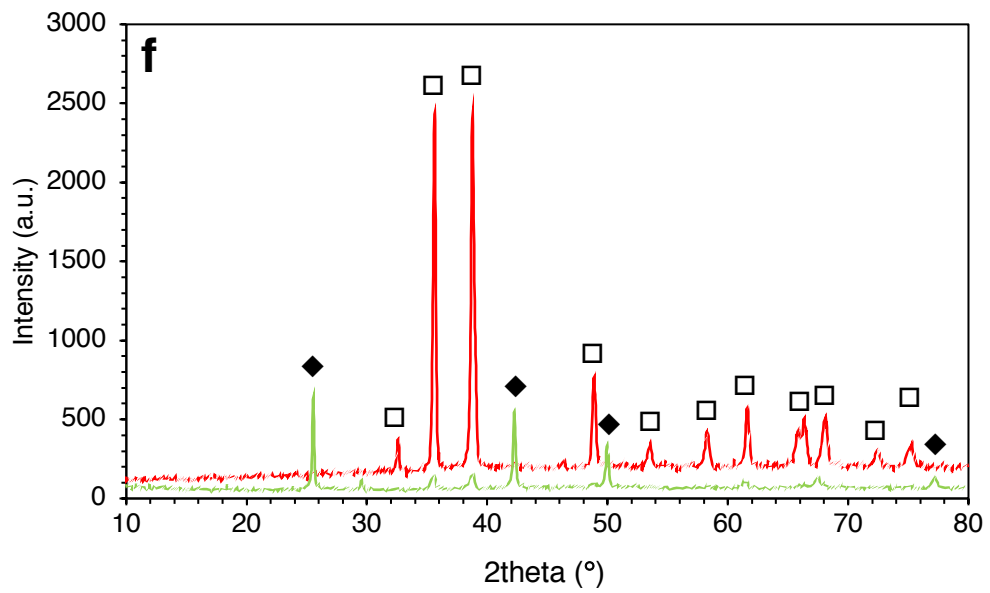
Samples of resins were contacted with various iodine-containing solutions and equilibrated, using the same batch conditions as described in the main research article. In all contact solutions, initial $[I^-]$ was 1.00 g.L^{-1} . The NaI/I₂ contact solution contained 6 molar equivalents I₂. The NaI/cocontaminants solution contained 10 molar equivalents of nitrate and molybdate.

The spent resin samples (~0.5 g) were placed in silica crucibles and heated to either 350 or $600 \pm 25^\circ\text{C}$ in a Vecstar ashing furnace, with temperature maintained for >1 hr. Samples were removed from the crucibles and analysed by powder XRD, as described in the main research article. In some cases, the crucible was broken into fragments and analysed using bulk sample holders.

Results

Crystalline species are identified as follows: \blacklozenge = CuI, \square = CuO, \circ = Cu₂O, \blacktriangledown = SiO₂, \star = CuMoO₄.





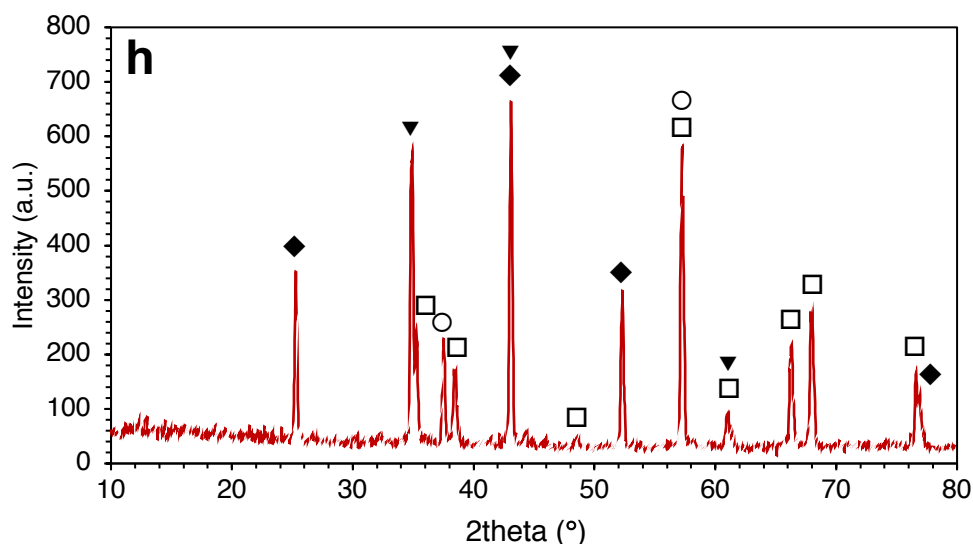


Figure S16. X-ray diffractograms for resin samples treated with various iodine-containing solutions. Green lines = samples heated to 350°C. Red lines = samples heated to 600°C (a) M4195 + iodide, (b) M4195 + iodide + iodine, (c) MTS9850 + iodide, (d) MTS9850 + iodide + iodine, (e) M4195-Cu + iodide, (f) M4195-Cu + iodide + iodine, (g) M4195-Cu + iodide + cocontaminants, (h) M4195-Cu + iodide + iodine (used silica crucible).

References

- [1] T.D.C. Company, DOWEX M4195 Chelating resin for copper, nickel, and cobalt processing in, 2019.
- [2] K.Y. Foo, B.H. Hameed, Insights into the modeling of adsorption isotherm systems, *Chemical Engineering Journal*, 156 (2010) 2-10.
- [3] M. Eriksson, I. Lundstrom, L.G. Ekedahl, A model of the Temkin isotherm behavior for hydrogen adsorption at Pd-SiO₂ interfaces, *Journal of Applied Physics*, 82 (1997) 3143-3146.
- [4] A.A. Inyinbor, F.A. Adekola, G.A. Olatunji, Kinetics, isotherms and thermodynamic modeling of liquid phase adsorption of Rhodamine B dye onto *Raphia hookerie* fruit epicarp, *Water Resources and Industry*, 15 (2016) 14-27.
- [5] P.U. Singare, Performance Based Evaluation of Industrial Grade Resins Duolite ARA-9366 and Duolite A-368 *Chemistry in Industry*, 63 (2014) 245-252.
- [6] P. Mao, Y. Liu, Y. Jiao, S.W. Chen, Y. Yang, Enhanced uptake of iodide on Ag@Cu₂O nanoparticles, *Chemosphere*, 164 (2016) 396-403.
- [7] S.W. Liu, S.H. Kang, H.M. Wang, G.Z. Wang, H.J. Zhao, W.P. Cai, Nanosheets-built flowerlike micro/nanostructured Bi₂O_{2.33} and its highly efficient iodine removal performances, *Chemical Engineering Journal*, 289 (2016) 219-230.
- [8] X.Y. Zhang, P. Gu, X.Y. Li, G.H. Zhang, Efficient adsorption of radioactive iodide ion from simulated wastewater by nano Cu₂O/Cu modified activated carbon, *Chemical Engineering Journal*, 322 (2017) 129-139.
- [9] G. Lefevre, M. Alnot, J.J. Ehrhardt, J. Bessiere, Uptake of iodide by a mixture of metallic copper and cupric compounds, *Environmental Science & Technology*, 33 (1999) 1732-1737.
- [10] H.F. Zhang, X.L. Gao, T. Guo, Q. Li, H.N. Liu, X.S. Ye, M. Guo, Z.J. Wu, Adsorption of iodide ions on a calcium alginate-silver chloride composite adsorbent, *Colloids and Surfaces a-Physicochemical and Engineering Aspects*, 386 (2011) 166-171.

- [11] D.N.T. Barton, T.J. Robshaw, O. Okusanya, D. Kim, S.E. Pepper, C.A. Sharrad, M.D. Ogden, Remediation of radioiodine using polyamine anion exchange resins, *Journal of Industrial and Engineering Chemistry*, 78 (2019) 210-221.
- [12] G.Y. Yan, T. Viraraghavan, M. Chen, A new model for heavy metal removal in a biosorption column, *Adsorption Science & Technology*, 19 (2001) 25-43.
- [13] J.T.M. Amphlett, C.A. Sharrad, R.I. Foster, M.D. Ogden, Ethylenediamine Functionalised Ion Exchange Resin for Uranium Recovery from Acidic Mixed Sulfate-Chloride Media: Initial Column Loading Studies, *Journal of the Southern African Institute of Mining and Metallurgy*, 118 (2018) 1521-1527.
- [14] T.J. Robshaw, R. Dawson, K. Bonser, M.D. Ogden, Towards the implementation of an ion-exchange system for recovery of fluoride commodity chemicals. Kinetic and dynamic studies *Chemical Engineering Journal*, 367 (2019) 149-159.
- [15] K.H. Chu, Fixed bed sorption: Setting the record straight on the Bohart-Adams and Thomas models, *Journal of Hazardous Materials*, 177 (2010) 1006-1012.
- [16] J.H.S. Green, W. Kynaston, H.M. Paisley, VIBRATIONAL SPECTRA OF MONOSUBSTITUTED PYRIDINES, *Spectrochimica Acta*, 19 (1963) 549-564.
- [17] M.S. Refat, H. Al Didamony, K.M. Abou El-Nour, L. El-Zayat, Synthesis and spectroscopic characterization on the tri-iodide charge transfer complex resulted from the interaction between morpholine as donor and iodine sigma-acceptor, *Journal of Saudi Chemical Society*, 14 (2010) 323-330.
- [18] L.Y. Wang, Q.Y. Chen, J. Huang, K. Wang, C.J. Feng, Z.R. Gen, Synthesis, characterization, and bioactivities of copper complexes with N-substituted Di(picoly)amines, *Transition Metal Chemistry*, 34 (2009) 337-345.